Hexagonal silicon–germanium nanowire branches with tunable composition

A Li, H I T Hauge, M A Verheijen, E P a M Bakkers, R T Tucker, L Vincent, C Renard

PAPER • **OPEN ACCESS**

Hexagonal silicon−germanium nanowire branches with tunable composition

To cite this article: A Li *et al* 2023 *Nanotechnology* **34** 015601

OPEN ACCESS
IOP Publishing
Nanotechnology

Nanotechnology **34** (2023) 015601 (8pp) https://doi.org/10.1088/1361-6528/ac9317

Hexagonal silicon−germanium nanowire branches with tunable composition

A Li[1], H I T Hauge[1], M A Verheijen[1,2], E P A M Bakkers[1], R T Tucker[1,3], L Vincent[4] and C Renard[4]

[1] Department of Applied Physics, TU Eindhoven, Den Dolech 2, 5612 AZ Eindhoven, The Netherlands
[2] Eurofins Materials Science, High Tech Campus 11, 5656 AE Eindhoven, The Netherlands
[3] Department of Electrical & Computer Engineering, University of Alberta, Edmonton, Alberta T6G 2V4, Canada
[4] Université Paris-Saclay, CNRS, Centre de Nanosciences et de Nanotechnologies, F-91120, Palaiseau, France

E-mail: ebakkers@tue.nl

Received 19 June 2022, revised 15 September 2022
Accepted for publication 20 September 2022
Published 12 October 2022

Abstract

Hexagonal SiGe-2H has been recently shown to have a direct bandgap, and holds the promise to be compatible with silicon technology. Hexagonal Si and Ge have been grown on an epitaxial lattice matched template consisting of wurtzite GaP and GaAs, respectively. Here, we present the growth of hexagonal Si and SiGe nanowire branches grown from a wurtzite stem by the vapor−liquid−solid growth mode, which is substantiated by *in situ* transmission electron microscopy. We show that the composition can be tuned through the whole range of stoichiometry from Si to Ge, and the possibility to realize Si and SiGe heterostructures in these branches.

Supplementary material for this article is available online

Keywords: nanowire, SiGe, hexagonal, crystal growth, 2H

(Some figures may appear in colour only in the online journal)

1. Introduction

Silicon (Si) and germanium (Ge) normally crystallize in the diamond cubic crystal structure, but are expected to exhibit interesting properties when grown in the hexagonal 2H structure. It has been predicted that hexagonal $Si_{1-x}Ge_x$ has a direct band gap at the Γ-point which is tunable in the range 0.3−0.7 eV [1–7], for $1.0 > x > 0.65$. This emission range is interesting for a broad range of applications, including telecommunication, LiDAR, and chemical sensing. In addition, hexagonal SiGe in the shape of nanowires is expected to have beneficial thermoelectric properties; calculations predict that the thermal conductivity of the hexagonal 2H phase of Silicon is almost a factor of 2 lower than that of cubic Si [8].

Hexagonal $Si_{1-x}Ge_x$ is a metastable material and does therefore not occur naturally. Although it is a challenge to fabricate this material synthetically, it can be forced in the hexagonal phase in nanosized materials [9–19], and one of the outstanding challenges is to increase the volume of the material. Single-crystalline hexagonal Si, Ge, and SiGe alloys have recently been reported in a nanowire (NW) core/shell geometry using a wurtzite III–V core wire as an epitaxial template [20–24]. This method has been successful for demonstrating the optical properties [24] but also has some drawbacks: (1) the group V element from the core material can be incorporated in the SiGe shell during growth [25] (2) I_3 planar stacking faults have recently been observed in SiGe shells [26], (3) and due to the large dimensions, lattice matching requirements are similar as for bulk materials, limiting the possiblities of growing SiGe heterostructures.

III–V nanowires with the wurtzite or cubic crystal structure can be grown directly from a Au catalyst particle, but this does not work for hexagonal SiGe when grown in the $\langle 111\rangle_C/\langle 0001\rangle_H$

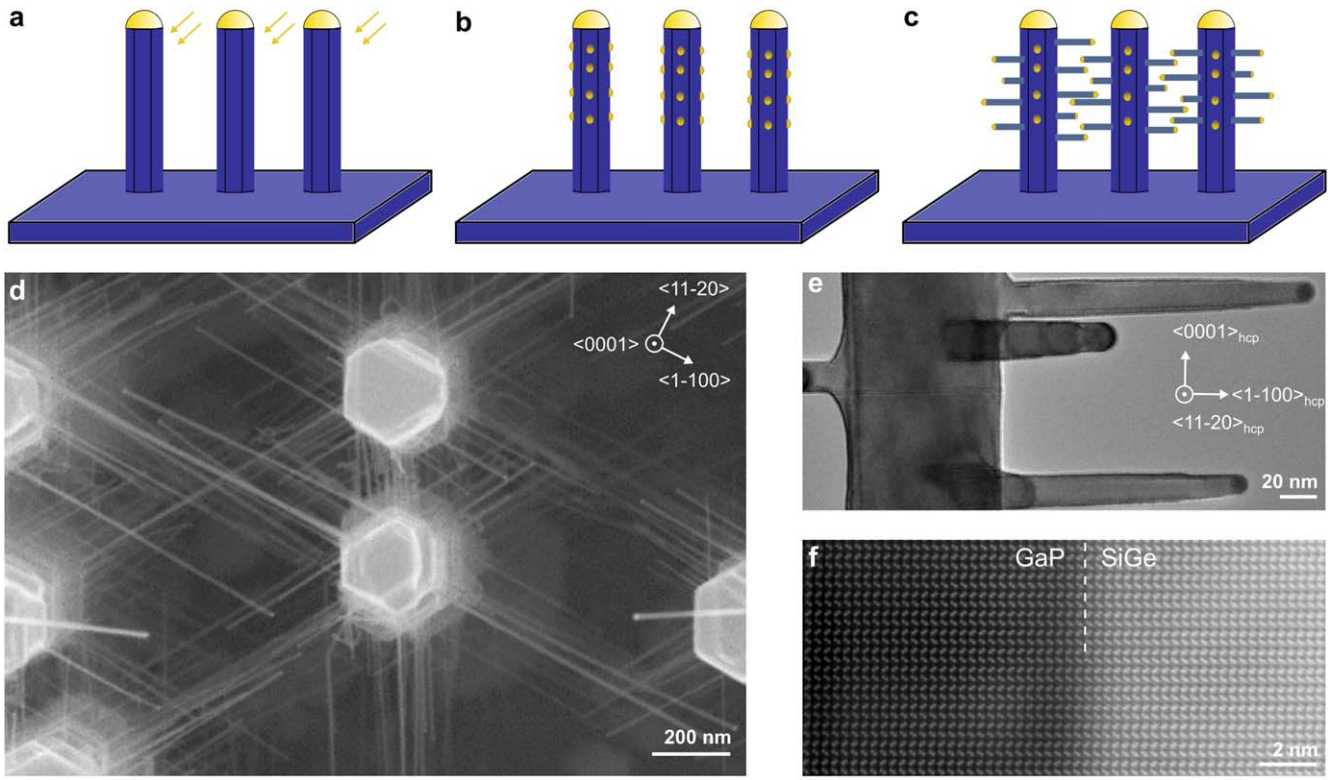

Figure 1. Growth of hexagonal SiGe NW branches on a wurtzite GaP stem. (a) Deposition of a Au layer on the sidewall of WZ GaP NW trunks followed by (b) Au droplet formation through annealing and finally, (c) VLS growth of branches by precursor introduction; (d) top-view SEM image of $Si_{0.64}$ $Ge_{0.36}$ branches; (e) side-view TEM image of the branches grown on the trunk. (f) High-resolution HAADF-STEM image showing the interface between the GaP trunk and the SiGe branch illustrating the epitaxial growth.

direction, since the system always crystallizes in the cubic phase. In this work, we report on the growth of single crystalline hexagonal SiGe nanowires with full compositional control along a ⟨1–100⟩ growth direction. We utilize the crystal structure transfer method [20] which has been employed successfully in the past to make hexagonal Si and $Si_{1-x}Ge_x$ shells [20–24]. But, in this case, we add an additional step by positioning Au particles on the sidewalls of the hexagonal core/shell NW and commence vapor −liquid−solid (VLS) growth of NWs, which resemble multiple branches growing out of a tree trunk. Branched nanowire growth has already been reported before [27–32]. In our case, the epitaxial growth on the wurtzite core wire enforces all the SiGe branches to grow in the hexagonal phase and an arbitrarily long NW can be produced. Due to the small dimensions of these branch wires, strain relaxation allows the fabrication of SiGe heterostructures. Moreover, optoelectronic or thermoelectric devices are more easily fabricated with the simple wire geometry as compared to the thick core/shell wires [20–24]. We note that hexagonal SiGe wires can, in principle, also be grown from a planar hexagonal substrate by the VLS mechanism; the challenge is to identify a suitable substrate.

2. Results

In this work we use wurtzite GaP (GaAs) core wires as epitaxial templates, which are almost lattice matched to Si (Ge). We illustrate the general principle of the branch growth process using a wurtzite GaP core in figure 1. We note here that the growth process is independent of the SiGe composition and the use of GaP or GaAs as trunk wires. Vertical hexagonal GaP NW trunks are grown from an array of 6 nm thick Au islands in 100 nm diameter mask openings defined by nanoimprint lithography (figure 1(a)) [33, 34]. From x-ray diffraction and transmission electron microscopy (TEM) studies we know that the GaP NWs have the hexagonal crystal structure and are basically free of defects (less than 1 SF μm^{-1}) [33, 34]. On the GaP NW sidewalls a second generation of Au catalyst particles is deposited by thermal evaporation under a 45° incidence angle (figure 1(b)). The side facets are then utilized as a substrate in order to epitaxially grow hexagonal $Si_{1-x}Ge_x$ ($0 \leqslant x \leqslant 1$) branches (figure 1(c)). In figure 1(d) a top-view scanning electron microscopy (SEM) image of the sample after growth of $Si_{0.64}Ge_{0.36}$ branches is shown. All Si:Ge ratios mentioned in the text have been determined using quantified STEM-EDX spectra. The absolute quantification of this ratio was calibrated against atom probe tomography in an earlier paper [24]. The cross section of the GaP NW exhibits a hexagonal shape with $\{11\bar{2}0\}$ side facets. The SiGe branches grow in six equivalent $\langle 1\bar{1}00\rangle$ azimuthal directions parallel to the facets. From the TEM image in figure 1(e) it is clear that all branches grow perpendicular to the long axis of the GaP nanowire trunk. In addition, the absence of diffraction contrast in the wires shows that these branches are single crystalline. In figure 1(f), we present a high-resolution scanning high-angle annular dark field scanning TEM (HAADF STEM) image showing the perfect epitaxial connection between the trunk and

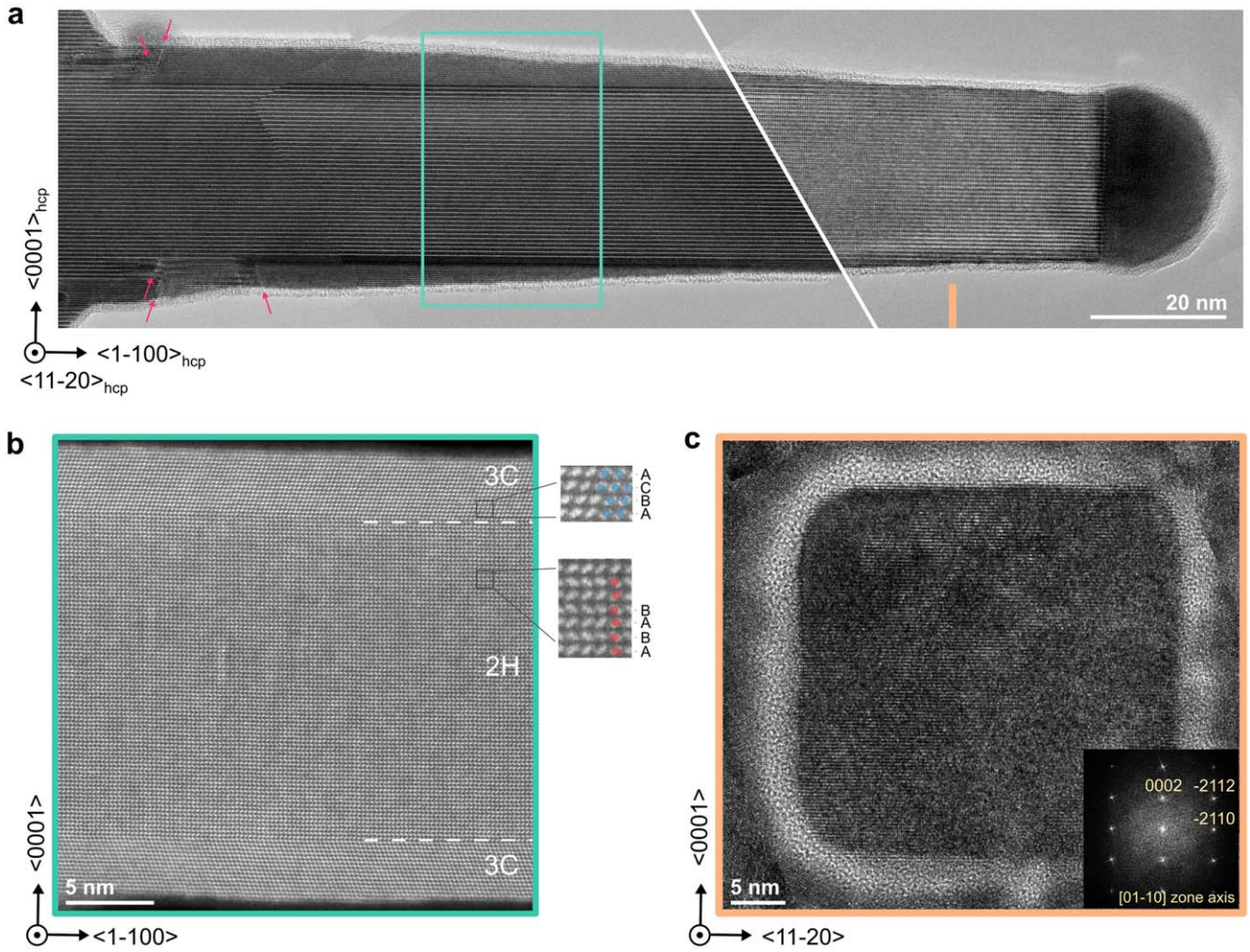

Figure 2. Structural characterization of SiGe branches. (a) Stitched HRTEM images of a defect-free core $Si_{0.46}Ge_{0.54}$ hexagonal branch. Defects in the shell are indicated by arrows (b) high-resolution HAADF-STEM image of a part of the branch in (a) illustrating the hexagonal core and the cubic layer on top and bottom of the branch taken along the $\langle 11\bar{2}0\rangle$ zone axis. (c) Cross-sectional HRTEM image of a branch taken along the $\langle 1\bar{1}00\rangle$ zone axis. In the inset a FFT (=Fast Fourier Transform) of the HR image is shown.

the branch. The characteristic 'dumbbells' of the hexagonal 2H crystal structure are evident, no defects are visible, while the contrast between GaP and SiGe is well discernable. The perfect epitaxy displays that the branch-growth method enables a defect-free interface, where the limited diameter of the branches ensures elastic strain relaxation at the base of the branch.

We now continue to study the structural properties of the branches in more detail by high resolution TEM of SiGe branches in figure 2. The HRTEM image in figure 2(a) is taken along the $\langle 11\bar{2}0\rangle$ zone axis which allows to discriminate between the cubic and hexagonal crystal phase [19], and shows a tapered branch. The core of the branch, which was grown by the VLS mechanism, displays ABAB stacking, as highlighted in figure 2(b), which signifies the hexagonal crystal structure, without planar defects. For a branch growing in the $\langle 1\bar{1}00\rangle$ direction, i.e. orthogonal to the ABAB stacking sequence, stacking faults cannot be formed perpendicular to the growth direction, and the crystal structure cannot be switched to the cubic phase. The observed tapering is partly due to simultaneous vapor−solid (VS) growth on the {0002} side facets on top and on the bottom of the branch as will be discussed below using the *in situ* TEM studies. This partial shell displays the diamond 3C crystal structure, visualized by ABCABC stacking of the crystal planes in figure 2(b). Crystal defects in the shell are recognizable close to the base of the branch, at the point where the cubic layers of the shell meet the hexagonal layers of the trunk. This implies that the shell growth originates from the nucleation of new layers on the {0002} side facets themselves, rather than by extending shell layers from the hexagonal trunk.

To substantiate the single-crystalline nature of the hexagonal SiGe branches, we have prepared cross-sectional cuts of the branches by using a focused ion beam (FIB). In figure 2(c) a HRTEM image of a cross-section of a branch is shown. There are no stacking faults or other defects visible within the structure. The cross-sectional shape of the branches, shown in figure 2(c), is rectangular, resulting from the 2-fold crystal symmetry around the $\langle 1\bar{1}00\rangle$ crystal axis. The core of the branch has the hexagonal crystal structure, which is extended to the $\{11\bar{2}0\}$ side facets of the branch by VS growth; we note that in the $\langle 11\bar{2}0\rangle$ direction, planar stacking faults cannot be formed and therefore the crystal structure of the shell adopts that of the core NW. As mentioned before,

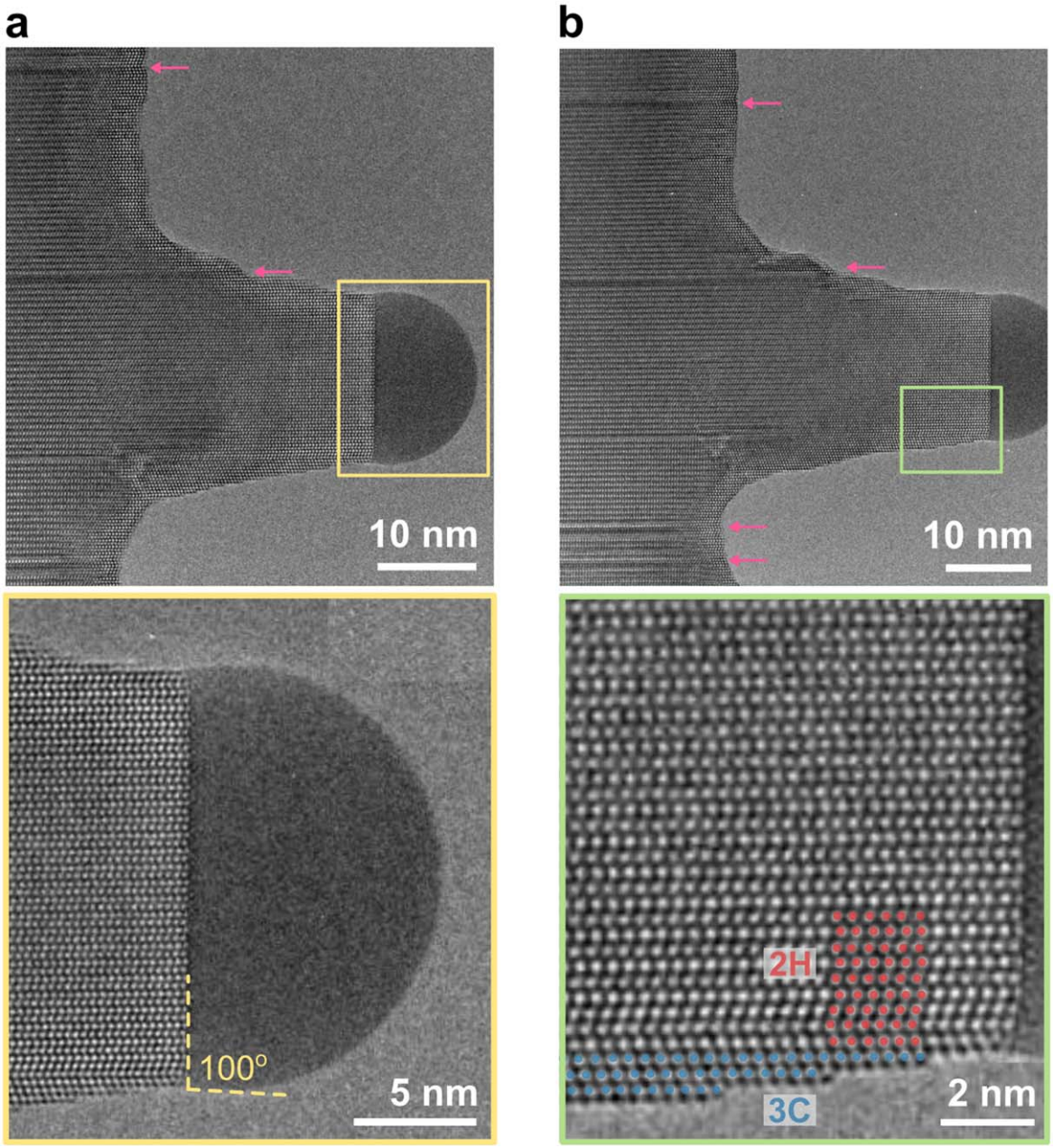

Figure 3. HRTEM *in situ* micrographs of a hexagonal Ge branch. (a), (b) Snapshots of the growth of a hexagonal Ge branch from Video1 (see supplementary information). Stacking faults, indicated by the arrows, are transferred from the GaAs core into the Ge. (a) Inset: enlarged view of the catalyst/NW interface, showing a flat interface and a contact angle of 100°. (b) Inset: the VLS growth of the central hexagonal Ge branch is highlighted in red while the VS growth of a cubic Ge-3C on {0002} sidewalls is highlighted in blue.

VS growth in the ⟨0001⟩ directions (top and bottom) results in the formation of the cubic crystal structure shell. Upon imaging along the $\langle 1\bar{1}00\rangle$ zone axis these two different crystal structures cannot be distinguished [19].

We have investigated the growth of Ge branches on wurtzite GaAs trunk nanowires using *in situ* TEM. The video (see supplementary information Video1 (available online at stacks.iop.org/NANO/34/015601/mmedia)) shows a Ge branch with the hexagonal crystal structure, imaged along a $\langle 11\bar{2}0\rangle$ zone axis, which grows epitaxially on the GaAs trunk nanowire by the Au-catalyzed VLS mechanism in the $\langle 1\bar{1}00\rangle$ direction, similar to the *ex situ* experiments. Snapshots of the main features of the growth are shown in figures 3 and 4. One must note that GaAs trunks have {1100}-type sidewalls, and in that case, branches grow perpendicular to the side facets, conversely to the previous GaP case where branches grow parallel to the {11–20} side facets. At the beginning of the growth, the liquid droplet on the branch tip has a large wetting angle with respect to the (1−100) interface (approximately 105° on the video and a corresponding diameter of around 18.5 nm). This contact angle stabilizes around 96°–100° (see figure 3(a) inset) and is maintained during the growth (the diameter of 17.2 nm does not evolve from 98 s (figure 3(a)) to 175 s (figure 3(b))). The hexagonal crystal structure in the

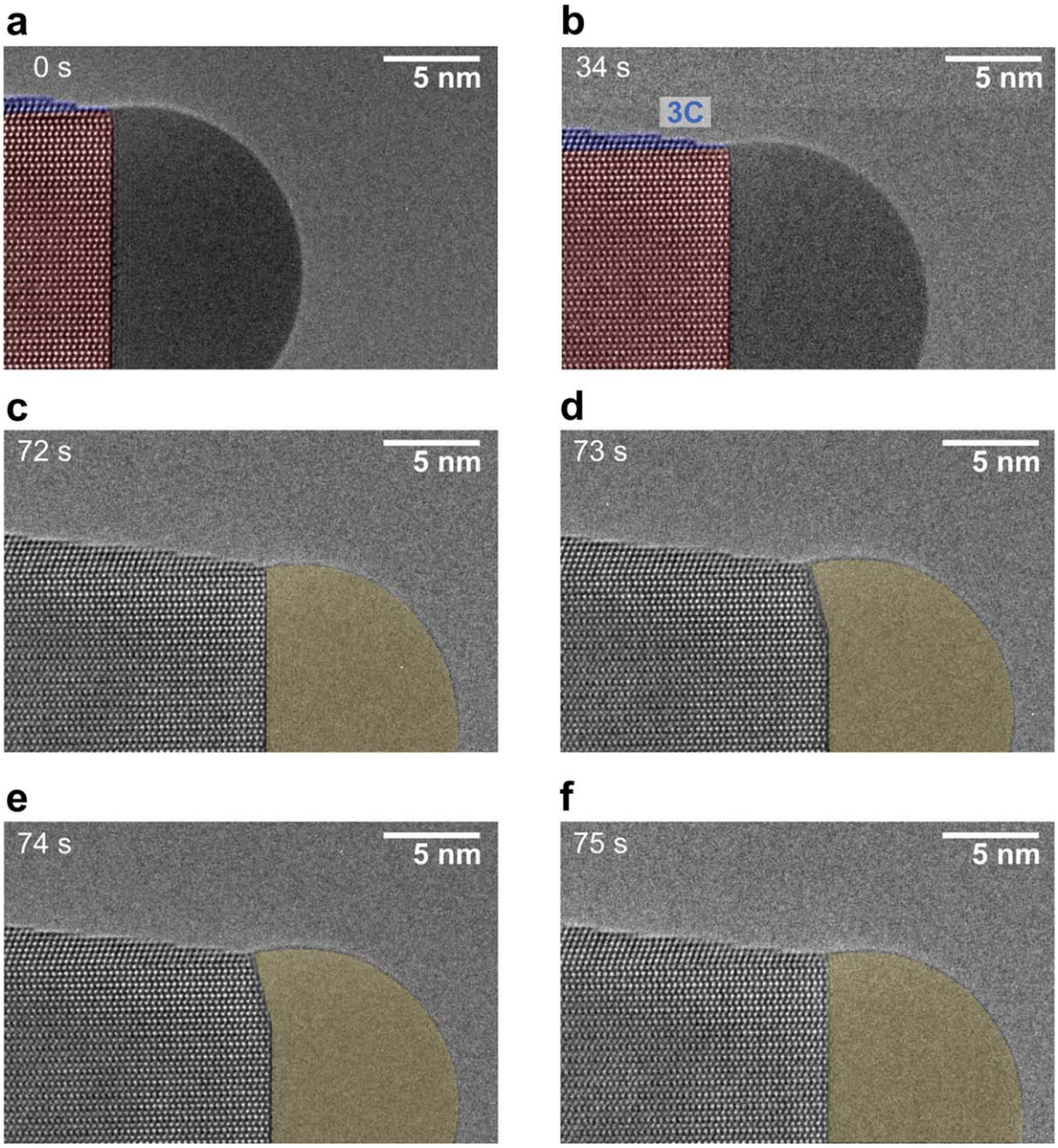

Figure 4. HRTEM snapshots of the triple-phase boundary (TPB). (a)–(f) Snapshots of the growth of a hexagonal Ge branch from Video2 (see supplementary information). (a), (b) The formation of a single cubic Ge layer at the TPB by the VLS mechanism. (c)–(f) show the evolution of the catalyst contact angle in conjunction to the formation of a truncated facet close to the TPB.

branch is formed by precipitation at the (1–100) liquid/solid interface by a layer-by-layer growth mode. At this moment, it is not clear if nucleation always occurs at the triple phase boundary (TPB) or at the liquid/solid interface. This question will be investigated in more detail in future studies. Any planar defect present in the GaAs template is replicated along the branch as pointed in figure 3. As observed in the *ex situ* studies, a cubic (3C) lateral Ge layer is grown on the top and bottom facets of the branch on the {0002} sides with several defects in this shell formed during the growth. We note that the axial (hexagonal) growth rate corresponds to 0.3 monolayers s^{-1} and the radial (cubic) rate is 0.05 monolayers s^{-1}.

From the video (see supplementary information Video2) and the corresponding enlarged snapshots shown in figures 4(a) and (b) it is clear that at least one monolayer of the cubic phase, highlighted in blue, nucleates at the TPB by the VLS mechanism. The cubic layer expands outwards by a VS mechanism in a layer-by-layer growth mode. The layers progress from the concave corner at the trunk-branch interface and then propagate towards the catalyst particle. The movies, and figures 4(c)–(f), also show that the liquid/solid interface between the catalyst and the branch is atomically flat in the centre, but truncated facets close to the TPB appear periodically as highlighted in blue in snapshots of the figures 4(c)–(f)

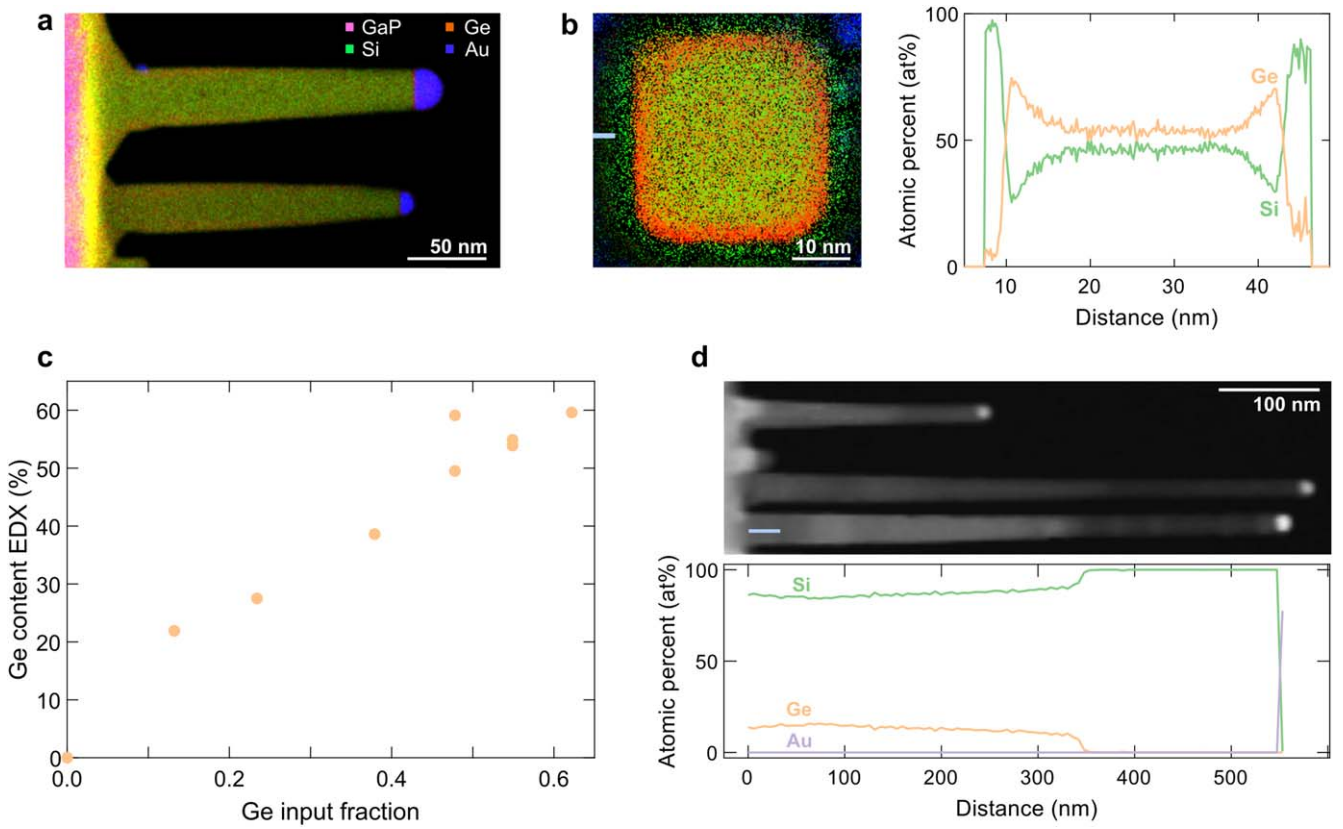

Figure 5. Compositional tuning of branches. (a) EDX map of $Si_{0.46}Ge_{0.54}$ branches showing the uniform composition, and the Ge-rich tapered shell. The yellow band between the core wire and the branch is due to an overlay of the elements. (b) Cross-sectional EDX map and a line profile of a branch taken along the $\langle 1\bar{1}00\rangle$ zone axis showing the $Si_{0.46}Ge_{0.54}$ composition in the centre and the Ge-enriched layer close to the surface. See supplementary information figure 1 for the oxygen line trace. (c) Incorporated Ge fraction as a function of the Ge precursor fraction in the gas phase. (d) HAADF STEM image of branches with a $Si_{0.80}Ge_{0.20}$/Si junction and the compositional profile along the entire branch depicted in the upper branch.

with variable angle of truncation. We note that the catalyst contact angle (defined as the angle between the droplet edge and the extrapolated planar solid-liquid interface to the edge) is 90° when there is no truncation and larger in case of a truncation. This particular point needs to be analysed in future experiments to understand the possible relationship between the truncation, the wetting angle, and the formation of the cubic layer at the TPB. An oscillatory truncation at the TPB has been observed before during the growth of Ge, and Si in the cubic $\langle 111\rangle$ direction and depends on the level of supersaturation in the catalyst [35, 36]. Here, using atomic resolution, we observe in the particular $\langle 1\bar{1}00\rangle$ growth direction that each truncation period corresponds to the formation of one Ge monolayer at the (1–100) liquid/solid interface. During the formation of the truncation, part of the already grown nanowire is dissolved in the catalyst particle and the dissolved Ge in the catalyst may serve to reach the required supersaturation for the formation of a new monolayer.

By developing a route for the growth of hexagonal Ge and Si NWs, we have laid the groundwork to further investigate the controllable growth of hexagonal $Si_{1-x}Ge_x$ compound nanowires, which is of interest since for $x > 0.65$ they should exhibit a direct band gap. These compound NWs have been grown at 620 °C, and x is controlled by the ratio of the input pressures of the precursors. In figure 5(a), we present an energy-dispersive x-ray (EDX) spectroscopy map to show the elemental composition of a number of SiGe branches, and measure a composition of $Si_{0.46}Ge_{0.54}$, which is close to the input ratio. The map further clarifies that the composition is uniform along the axis of the branch NW, but a Ge-rich tapered shell can be observed. In order to investigate the composition in the viewing direction that is parallel to the axis of the branch NW, we prepared a cross-sections of a branch. The cross-sectional EDX map in figure 5(b) shows that the composition of the branch NWs is uniform in the center, whereas there is a Ge rich outer shell of the hexagonal SiGe, surrounded by a SiO_2 outer shell. The Ge-enriched sub-surface layer could be explained by segregation due to preferential oxidation of Si at the surface [37], or by the different growth dynamics of VS compared to VLS growth; the non-uniform thickness of the Ge-enriched layer in figure 5(a) suggests the latter. We note that the formation of a SiO_x surface layer, eliminating dangling bonds and creating a wide bandgap capping, is probably beneficial for the optoelectronic properties of the branch NWs. In figure 5(c), we have plotted the Ge content incorporated into the SiGe branch, as determined by EDX spectroscopy, as a function of the input ratio of the Ge and Si precursors. With this fabrication methodology, it is possible to tune the composition of the hexagonal $Si_{1-x}Ge_x$ branch NWs in the full range. The flexibility that this fabrication method provides is further investigated by growing more complex

heterostructures in the same branch NW. In figure 5(d), A HAADF image shows a number of branch wires grown from the GaP trunk. A quantitative compositional line profile along a 0.5 μm long branch shows the variation in composition along the branch: starting with $Si_{0.80}Ge_{0.20}$ at the base of the branch and pure Si at the tip.

3. Conclusion

In conclusion, we have fabricated $Si_{1-x}Ge_x$ nanowires with the hexagonal crystal structure by growing them as epitaxial branches on a suitable substrate trunk NW. We show that it is possible to fabricate $Si_{1-x}Ge_x$ NWs throughout the whole stoichiometric range and even simple SiGe heterostructures. Future steps are to realize optically active quantum dots and simple opto-electronic devices of hexagonal Si and SiGe nanowires defined in the axial direction.

Acknowledgments

We would like to thank P J van Veldhoven for technical support at the MOVPE reactor, A Cavalli, L Gagliano, and M Y Swinkels for nanoimprint preparation, M J Brett for valuable discussions, and G Badawy for designing the figures. This work was supported by the Dutch Organization for Scientific Research (NWO-VICI 700.10.441), and the European Union's Horizon 2020 research and innovation program under grant agreement number 964191 (Opto Silicon). Solliance and the province of Noord-Brabant are acknowledged for funding the TEM facility. This project has received funding from the French National Research Agency (ANR) under the grant ANR-17-CE030–0014–01 (HEXSIGE). We acknowledge the ANR for funding the NANOMAX ETEM through the TEMPOS grant (10-EQPX-0050)). We acknowledge Odile Stephan leader of TEMPOS and Jean Luc Maurice manager of NANOMAX. We wish to particularly acknowledge Ileana Florea and Federico Panceira for the technical assistance during experiments. Thanks are due to the CIMEX at École polytechnique (Palaiseau, France) for hosting the NANOMAX microscope.

Data availability statement

The data that support the findings of this study will be openly available following an embargo at the following URL/DOI: https://doi.org/10.5281/zenodo.6664593. Data will be available from 19 July 2022.

Experimental details

The wurtzite trunk GaP wires have been grown following references [31, 32] in a close-coupled showerhead reactor by Aixtron. The branches have been grown in the same MOVPE reactor at a total pressure of 50 mbar, and a total gas flow of 6200 sccm. After deposition of the Au particles on the GaP trunk wires, the samples are annealed at 710 °C for 1 min. For the growth of the branches the samples are cooled to 650 °C and exposed to 1% GeH_4/H_2 and 1% Si_2H_6/H_2. The total group IV input flow is between 190 and 300 sccm.The input flux ratio of the precursors determines the chemical composition of the branches. The branches are grown for 6 or 6 and a half minutes.

For the TEM measurements, two different sample preparation methods were used. In the standard side-view analysis, branched nanowires are mechanically transferred to a holey carbon TEM grid. For the cross-sectional TEM studies, nanowires are prepared using a FEI Nova Nanolab 600i dual beam system. In both cases, high-resolution TEM and scanning TEM (STEM) analyses are conducted using a JEM ARM200F probe-corrected TEM operated at 200 kV. Energy dispersive x-ray (EDX) spectroscopy measurements are carried out using the same microscope equipped with a 100 mm^2 EDX silicon drift detector.

For *in situ* dynamical HRTEM observations, we have utilized Au-catalyzed wurtzite GaAs nanowires as a template for the growth of Ge-2H branches. Observations are carried out using a Cs-corrected Titan environmental TEM (ETEM) operated at 300 kV. Movies are recorded using a Gatan US1000 camera at a rate of 4 fps. The images in the article are snapshots extracted from the videos. We use a Protochips FUSION sample holder with heating chips featuring a SiC membrane with nine holes of 10 μm diameter for the observation and providing uniform heating in the observation area. The growth of GaAs NWs is done using trimethylgallium (TMGa) and tertiarybutylarsine (TBAs) and catalysed Ge branches are grown using digermane (Ge_2H_6) diluted in H_2 (10% by volume). The mixture is then delivered to the microscope column by an injector connected near the pole piece.

For the growth of GaAs nanowires, Au nanoparticles are deposited by evaporation on the FUSION heating e-chips and then *in situ* annealed to generate Au nanodroplets. The growth is preformed at around 450 °C. The zinc blende to wurtzite phase transition is tuned by changing the V/III ratio during the growth with a pressure from 2×10^{-3} mbar to 1.10^{-2} mbar. After the growth of GaAs NWs, organometallics are simultaneously stopped. The tip Au droplets are destabilised by increasing the temperature rapidly. After the Au droplets have moved to the sidewall of the GaAs-w NW, diluted Ge_2H_6 is injected at 3 sccm and a pressure of around 8×10^{-3} mbar and VLS growth of the Ge branch is observed at around 330 °C.

Author contributions

RTT and EPAMB designed the *ex situ* experiments, LV and CR designed and conducted the *in situ* experiments. AL and HITH have grown the NWs *ex situ*, RTT and AL performed the NW sidewall Au deposition, MAV performed the *ex situ* TEM analysis of the NWs. AL, HITH, RTT, MAV and EPAMB contributed to the interpretation of the *ex situ* data, and LV analysed the data from in situ experiments. HITH, EPAMB, and LV wrote the manuscript. All authors discussed

the results and commented on the manuscript. LV and EPAMB supervised the project, and acquired the research funding that supported this study.

Notes

The authors declare no competing financial interest.

ORCID iDs

M A Verheijen https://orcid.org/0000-0002-8749-7755
E P A M Bakkers https://orcid.org/0000-0002-8264-6862
L Vincent https://orcid.org/0000-0002-9813-9259

References

[1] Joannopoulos J D and Cohen M L 1973 Electronic properties of complex crystalline and amorphous phases of Ge and Si: I. Density of states and band structures *Phys. Rev. B* **7** 2644–57
[2] De A and Pryor C E 2014 Electronic structure and optical properties of Si, Ge and diamond in the lonsdaleite phase *J. Phys.: Condens. Matter* **26** 45801
[3] Persson C and Janzén E 1998 Electronic band structure in hexagonal close-packed Si polytypes *J. Phys.: Condens. Matter* **10** 10549–55
[4] Rödl C, Furthmüller J, Suckert J R, Armuzza V, Bechstedt F and Botti S 2019 Accurate electronic and optical properties of hexagonal germanium for optoelectronic applications *Phys. Rev. Mater.* **3** 034602
[5] Jens Renè S, Claudia R, Jürgen F, Friedhelm B and Silvana B 2021 Efficient strain-induced light emission in lonsdaleite germanium *Phys. Rev. Mater.* **5** 024602
[6] Xavier C, Palummo M, Hauge H I T, Bakkers E P A M and Rurali R 2017 Optical emission in hexagonal SiGe nanowires *Nano Lett.* **17** 4753–8
[7] Wang Z, Zhang Z, Liu S, Robertson J and Guo Y 2021 Electronic properties and tunability of the hexagonal SiGe alloys *Appl. Phys. Lett.* **118** 172101
[8] Raya-Moreno M, Aramberri H, Seijas-Bellido J A, Cartoixà X and Rurali R 2017 Thermal conductivity of hexagonal Si and hexagonal Si nanowires from first-principles *Appl. Phys. Lett.* **111** 032107
[9] Jennings H M and Richman M H 1976 A hexagonal (Wurtzite) form of silicon *Science* **193** 1242–3
[10] Wentorf R H and Kasper J S 1963 Two new forms of silicon *Science* **139** 338–9
[11] Qiu Y, Bender H, Richard O, Kim M-S, Van Besien E, Vos I, de Potter de ten Broeck M, Mocuta D and Vandervorst W 2015 Epitaxial diamond-hexagonal silicon nano-ribbon growth on (001) silicon *Sci. Rep.* **5** 12692
[12] Vincent L, Patriarche G, Hallais G, Renard C, Gardès C, Troadec D and Bouchier D 2014 Novel heterostructured ge nanowires based on polytype transformation *Nano Lett.* **14** 4828–36
[13] Fontcuberta I Morral A, Arbiol J, Prades J D, Cirera A and Morante J R 2007 Synthesis of silicon nanowires with wurtzite crystalline structure by using standard chemical vapor deposition *Adv. Mater.* **19** 1347–51
[14] Xiao S-Q and Pirouz P 1992 On diamond-hexagonal germanium *J. Mater. Res.* **7** 1406–12
[15] Lopez F J, Hemesath E R and Lauhon L J 2009 Ordered stacking fault arrays in silicon nanowires *Nano Lett.* **9** 2774–9
[16] Bandet J, Despax B and Caumont M 2002 Vibrational and electronic properties of stabilized wurtzite-like silicon *J. Phys. D: Appl. Phys.* **35** 234–9
[17] Liu X and Wang D 2009 Kinetically-induced hexagonality in chemically grown silicon nanowires *Nano Res.* **2** 575–82
[18] Pirouz P, Chaim R, Dahmen U and Westmacott K H 1990 The martensitic transformation in silicon: I. Experimental observations *Acta. Metall. Mater.* **38** 313–22
[19] den Hertog M I, Cayron C, Gentile P, Dhalluin F, Oehler F, Baron T and Rouviere J L 2012 Hidden defects in silicon nanowires *Nanotechnology* **23** 25701
[20] Algra R E, Hocevar M, Verheijen M A, Zardo I, Immink G G W, van Enckevort W J P, Abstreiter G, Kouwenhoven L P, Vlieg E and Bakkers E P A M 2011 Crystal structure transfer in core/shell nanowires *Nano Lett.* **11** 1690–4
[21] Hauge H I T *et al* 2015 Hexagonal silicon realized *Nano Lett.* **15** 5855–60
[22] Hauge H I T, Conesa-Boj S, Verheijen M A, Koelling S and Bakkers E P A M 2017 Single-crystalline hexagonal silicon −germanium *Nano Lett.* **17** 85–90
[23] Yizhen Ren P, Leubner M A, Verheijen J E M, Haverkort and Erik P A M B 2019 Hexagonal silicon grown from higher order silanes *Nanotechnology* **30** 295602
[24] Fadaly E M T *et al* 2020 Direct-bandgap emission from hexagonal Ge and SiGe alloys *Nature* **580** 205–9
[25] Kölling S, Plantenga R C, Hauge H I T, Ren Y, Li A, Verheijen M A, Conesa Boj S, Assali S, Koenraad P M and Bakkers E P A M 2016 Impurity and defect monitoring in hexagonal Si and SiGe nanocrystals *ECS Trans.* **75** 751–60
[26] Fadaly E M T *et al* 2021 Unveiling planar defects in hexagonal group IV materials *Nano Lett.* **21** 3619–25
[27] Dick K A, Deppert K, Larsson M W, Mårtensson T, Werner S, Wallenberg L R and Samuelson L 2004 Synthesis of branched 'nanotrees' by controlled seeding of multiple branching events *Nat. Mater.* **3** 380–4
[28] Dick K A *et al* 2007 The morphology of axial and branched nanowire heterostructures *Nano Lett.* **7** 1817–22
[29] Wang D, Qian F, Yang C, Zhong Z and Lieber C M 2004 Rational growth of branched and hyperbranched nanowire structures *Nano Lett.* **4** 871–4
[30] Beaudry A L, Tucker R T, LaForge J M, Taschuk M T and Brett M J 2012 Indium tin oxide nanowhisker morphology control by vapour–liquid–solid glancing angle deposition *Nanotechnology* **23** 105608
[31] Beaudry A L, LaForge J M, Tucker R T, Sorge J B, Adamski N L, Li P, Taschuk M T and Brett M J 2014 Directed branch growth in aligned nanowire arrays *Nano Lett.* **14** 1797–803
[32] Kennedy T, Bezuidenhout M, Palaniappan K, Stokes K, Brandon M and Ryan K M 2015 Nanowire heterostructures comprising germanium stems and silicon branches as high-capacity Li-Ion anodes with tunable rate capability *ACS Nano* **9** 7456–65
[33] Assali S *et al* 2013 Direct band gap wurtzite gallium phosphide nanowires *Nano Lett.* **13** 1559–63
[34] Assali S, Gagliano L, Oliveira D S, Verheijen M A, Plissard S R, Feiner L F and Bakkers E P A M 2015 Exploring crystal phase switching in GaP nanowires *Nano Lett.* **15** 8062–9
[35] Gamalski A D, Ducati C and Hofmann S 2011 Cyclic supersaturation and triple phase boundary dynamics in germanium nanowire growth *J. Phys. Chem. C* **115** 4413–7
[36] Chen C-Y, Tersoff J, Hillerich K, Reuter M C, Park J H, Kodambaka S, Stach E A and Ross F M 2011 Periodically changing morphology of the growth interface in Si, Ge, and GaP nanowires *Phys. Rev. Lett.* **107** 025503
[37] Brewer W M *et al* 2017 Lateral Ge diffusion during oxidation of Si/SiGe fins *Nano Lett.* **17** 2159–64